Unclassified
SECURITY CLASSIFICATION OF THIS PAGE

(2)

DTIC ELECTE AUG 08 1990 D

DTIC FILE COPY

REPORT DOCUMENTATION PAGE

AD-A224 949

1b. RESTRICTIVE MARKINGS

3. DISTRIBUTION/AVAILABILITY OF REPORT
Approved for public release:
Distribution unlimited

4. PERFORMING ORGANIZATION REPORT NUMBER(S)
4

5. MONITORING ORGANIZATION REPORT NUMBER(S)
4

6a. NAME OF PERFORMING ORGANIZATION
Department of Chemistry
Rice University, Houston

6b. OFFICE SYMBOL (If applicable)

7a. NAME OF MONITORING ORGANIZATION
Office of Sponsored Research
Rice University, P.O. Box 2692

6c. ADDRESS (City, State, and ZIP Code)
Houston, Texas 77251

7b. ADDRESS (City, State, and ZIP Code)
Houston, Texas 77252

8a. NAME OF FUNDING/SPONSORING ORGANIZATION
Office of Naval Research

8b. OFFICE SYMBOL (If applicable)

9. PROCUREMENT INSTRUMENT IDENTIFICATION NUMBER
N00014-88-K-0553

8c. ADDRESS (City, State, and ZIP Code)
Chemistry Division
800 N. Quincy Street
Arlington, VA 22217-5000

10. SOURCE OF FUNDING NUMBERS

PROGRAM ELEMENT NO.	PROJECT NO.	TASK NO	WORK UNIT ACCESSION NO
412M007			

11. TITLE (Include Security Classification)
Ammonia Chemisorption Studies on Silicon Cluster Ions

12. PERSONAL AUTHOR(S)
J. M. Alford, R. T. Laaksonen, and R. E. Smalley

13a. TYPE OF REPORT	13b. TIME COVERED	14. DATE OF REPORT (Year, Month, Day)	15. PAGE COUNT
Interim/Technical	FROM _____ TO _____	July 23, 1990	43

16. SUPPLEMENTARY NOTATION
J. Chem. Phys. (1990)

17. COSATI CODES			18. SUBJECT TERMS (Continue on reverse if necessary and identify by block number)
FIELD	GROUP	SUB-GROUP	Surface chemistry; ammonia chemisorption; silicon cluster ions. (JES)

19. ABSTRACT (Continue on reverse if necessary and identify by block number)

Silicon clusters in the size range from 5 to 66 atoms were generated by laser vaporization in a supersonic nozzle and injected into the ion trap of a specially-designed Fourier transform ion cyclotron resonance apparatus. On the positively charged clusters ammonia chemisorption reaction rates were found to vary by over three orders of magnitude as a function of cluster size, with clusters of 21, 25, 33, 39, and 45 atoms being particularly unreactive, and cluster 43 being the most reactive. For the negative cluster ions, 43 was the only cluster found to react substantially. Although the reaction behaviour of many clusters clearly indicated that several structural isomers were present with different reaction rates, the strikingly low net reactivity of such clusters as 39 and 45 provides evidence that they have effectively crystallized into a single specially stable form.

Keywords:

20. DISTRIBUTION/AVAILABILITY OF ABSTRACT
☒ UNCLASSIFIED/UNLIMITED ☐ SAME AS RPT. ☐ DTIC USERS

21. ABSTRACT SECURITY CLASSIFICATION
Unclassified

22a. NAME OF RESPONSIBLE INDIVIDUAL
Richard E. Smalley

22b. TELEPHONE (Include Area Code)
(713) 527-4845

22c. OFFICE SYMBOL

DD FORM 1473, 84 MAR

83 APR edition may be used until exhausted.
All other editions are obsolete.

SECURITY CLASSIFICATION OF THIS PAGE
Unclassified

OFFICE OF NAVAL RESEARCH

CONTRACT N00014-88-K-0553

R&T Code 412m007

Technical Report No. 4

Ammonia Chemisorption Studies on Silicon Cluster Ions

by

J. M. Alford, R. T. Laaksonen, and R. E. Smalley

J. Chem. Phys. (1990)

Rice University
Department of Chemistry
Houston, Texas

July 23, 1990

ABSTRACT

Silicon clusters in the size range from 5 to 66 atoms were generated by laser vaporization in a supersonic nozzle and injected into the ion trap of a specially-designed Fourier transform ion cyclotron resonance apparatus. On the positively charged clusters ammonia chemisorption reaction rates were found to vary by over three orders of magnitude as a function of cluster size, with clusters of 21, 25, 33, 39, and 45 atoms being particularly unreactive, and cluster 43 being the most reactive. For the negative cluster ions, 43 was the only cluster found to react substantially. Although the reaction behaviour of many clusters clearly indicated that several structural isomers were present with different reaction rates, the strikingly low net reactivity of such clusters as 39 and 45 provides evidence that they have effectively crystallized into a single specially stable form.

J. Chem. Phys.
submitted July, 1990

AMMONIA CHEMISORPTION STUDIES ON SILICON CLUSTER IONS

J. M. Alford[a], R. T. Laaksonen, and R. E. Smalley

Rice Quantum Institute
and
Departments of Chemistry and Physics
Rice University
Houston, Texas 77251

a. Current Address: Tecmag Inc., 6006 Bellaire Blvd., Suite 117, Houston, Texas 77081.

ABSTRACT

Silicon clusters in the size range from 5 to 66 atoms were generated by laser vaporization in a supersonic nozzle and injected into the ion trap of a specially-designed Fourier transform ion cyclotron resonance apparatus. On the positively charge clusters ammonia chemisorption reaction rates were found to vary by over three orders of magnitude as a function of cluster size, with clusters of 21, 25, 33, 39, and 45 atoms being particularly unreactive, and cluster 43 being the most reactive. For the negative cluster ions, 43 was the only cluster found to react substantially. Although the reaction behavior many clusters clearly indicated that several structural isomers were present with different reaction rates, the strikingly low net reactivity of such clusters as 39 and 45 provides evidence that they have effectively crystallized into a single specially stable form.

I. INTRODUCTION

Several years ago in this journal we reported initial coarse indications that something appeared to be special about certain positive cluster ions of silicon[1]. This is a more complete account of such experiments, and is intended as well to serve as documentation of a major stage in the development of the FT-ICR technique for the study of clusters in general. In particular this is the first extensive discussion of the details of the implementation and extensive use of SWIFT, a powerful technique for the selective manipulation of cluster ions levitated in the superconducting magnetic field of an ICR trap. Extensive reaction studies of positive clusters of silicon are presented for all cluster sizes from 6 to 65 atoms, and for negative silicon clusters in the size range from 39 to 50.

II. EXPERIMENTAL

Figure 1 presents an overview of the apparatus used in these studies. Many of the details of this apparatus have been discussed in detail in previous publications[2-4], so we will review them only briefly here, except

where there have been significant changes. A pulsed supersonic beam of positive silicon cluster ions was made by laser vaporization of a rotating/translating silicon disc mounted on the side of a pulsed supersonic nozzle. For clusters smaller than 25 atoms in size, sufficient positive cluster ions were present in the supersonic jet using just the residual ionization left over from the laser vaporization event in the nozzle. For larger clusters, however, it was necessary to use an ArF excimer laser beam (6.4 eV) directed down the jet axis (the "Ionizing Laser" beam marked in Fig 1.) to regenerate ionization in the supersonic jet near the start of the expansion cone of the nozzle. Later experiments[5,6] have made it clear that use of an ionization laser for the production of the large clusters ions may have been a critical factor in at least partially annealing the clusters into well-formed structures[7,8].

The cluster ions were directed out of the supersonic beam with pulsed extraction stack at an energy of 660-710 eV and directed into the 6 T superconducting magnet of the FT-ICR apparatus where they were decelerated and trapped in the ICR cell. The details of this extraction and trapping operation were similar to that discussed before[2,4]. However, the 2-stage decelerator used previously was replaced by a much simpler single deceleration stage consisting of a 20 long stainless steel tube, 3.0 cm id joined at the end to a stainless steel disc-shaped electrode with a central 2.5 cm id. hole covered with a molybdenum mesh. Figure 2 shows a perspective view of this pulsed decelerator and the ICR cell electrodes, together with the pulsed extraction and cluster ion beam guiding optics.

The mesh-covered end electrode of the pulsed decelerator labelled "G1" in Fig. 2 was positioned 12 cm away from the center of the ICR cell. The critical electrode involved in selecting a particular mass range of clusters to be trapped is one we refer to as the "screen door". It is seen in Fig. 2, labelled G2, situated 1 cm away from G1. When the cluster ion packet to be trapped arrives at the middle of the pulsed decelerator tube, the voltage is dropped to -660 V. Since the cluster ions are inside the decel tube far away from the ends at this time, they experience no field until later when they drift through the grid G1. They are decelerated as they move toward the screen door grid G2.

The ICR trap used for these experiments consisted of a 15 cm long cylinder, 4.8 cm ID with the side walls divided into two opposing 120^{o} sectors for excitation and a pair of 60^{o} sectors for detection. The front and rear "doors" of the cell were flat discs with 2.5 cm id. open tubes, 2.5 cm long, for cluster ion injection and laser alignment. All electrodes of the ICR cell were made of copper electroplated with silver, with a thin layer of rhodium. As seen in Fig. 1, the ICR portion of the apparatus was pumped by a combination of turbopumps and cryopumps, providing a base pressure in the ICR cell in the low 10^{-9} torr range. The experiments reported in this work were performed with the ICR cell at 300 K.

During the cluster injection period of a typical experiment the side plates of the ICR cell were held at 0 V, the front door at 2 V and the rear door at 10 V. Under computer control as the desired cluster mass passed though the decelerator, the screen door, G2, was pulsed from 10 V to 0 V, permitting the original 660-710 eV spread of cluster ion energies decelerated to 0-50 eV to drift into the front door, the ions with over 2 eV energy passing into the ICR cell. Cluster ions with energies less than 10 eV will be reflected when they reach the rear door, but by the time they bounce back to the screen door it has been pulsed back to 10 V and these 2-8 eV clusters are trapped. After each injection shot a pulse of argon gas was injected into the region of the ICR cell, bringing the pressure up to $1x10^{-5}$ torr. Collisions of the trapped cluster ions with this argon gas starts the process of thermalizing the clusters, rapidly removing most of the axially-directed translational energy. This entire sequence of events was the replicated at a rate of 10 s^{-1} until the ICR cell was "full" -- usually on the order of 100 shots for the experiments reported here.

After the injection cycle was complete the clusters were further thermalized by exposure to $2x10^{-6}$ torr argon for 10 seconds, which corresponds to roughly 350 collisions at the Langevin rate. After a 2-3 second delay to allow the ICR cell pressure to drop below $5x10^{-8}$ torr, the clusters were then selectively ejected from the cell so that only the particular isotopic forms of interest were left. These were then rethermalized by a second exposure to argon (roughly 50 collisions), and then exposed to the reactant gas. The

resulting cluster mass distribution consisting of the remaining unreacted clusters and their reaction products was then detected by uniform coherent excitation of the cyclotron motion. Detection of the ICR transient then proceeded by sensitive measurement of the image currents flowing to the detector plates by a sensitive preamplifier (Stanford Research Systems SR560), followed by digitization of the heterodyned signal, and calculation of the Fourier transform.

Most of the details of the electronics and control aspects of this apparatus have been described elsewhere[2,4,7]. The sole exception is the computerized coherent excitation procedure which is described here in detail for the first time.

SELECTIVE EXCITATION AND EJECTION OF IONS -- "SWIFT"

One of the principal virtues of studying ion molecule chemistry in an ICR trap is that the cyclotron resonance frequency depends on the mass of the ion, and -- most importantly -- it is independent on the energy of the ion. In addition to permitting wide band detection of the mass spectrum at high resolution and sensitivity, this aspect of the physics of cyclotron motion provides a means of sorting through the contents of a mixture of ions in the trap, providing coherent cyclotron excitation to a mass-selected portion of the ions. This selective excitation can be used to detect only in a selected mass region, or to excite the cyclotron resonance to such a high amplitude that the ions collide with the side plates of the ICR cell and are therefore effectively swept away.

In cases such as the silicon cluster reaction studies to be discussed below where there are many isotopic variants of each cluster due to the substantial natural abundance of Si^{28}, Si^{29}, and Si^{30}, it is often difficult to sort out mass peaks due to the reaction products. Since this problem of discriminating reaction products from the initial cluster mass distribution is such a serious problem for metal and semiconductor cluster ions in general,

we have invested a major effort in developing selective rf sweeping technology as extensively as possible.

One obvious approach is simply to scan the frequency of the rf excitation to the ICR cell over the range of cyclotron resonances appropriate to the cluster mass range one wishes to sweep from the cell. The problem is that any finite duration rf sweep will contain frequency components outside the range intended. For example, the top panel of Figure 3 shows the measured rf power spectrum produced by a linear scan of rf frequency from 10.0 to 15.0 kHz in a time period of 30 milliseconds. Note the substantial oscillations in effective rf power as a function of frequency within the intended sweep range, and the significant tail of excitation outside of this range.

As first pointed out by Marshall and coworkers[9,10] there is an much more elegant solution to this problem than simply scanning the rf frequency from one point to another. If what one wants to do is craft a time domain voltage waveform which has uniform rf power in a certain frequency range, but zero rf power elsewhere, the most direct approach is then simply to take the inverse Fourier transform of the desired power spectrum and generate a voltage waveform from the resulting time domain data array using a fast digital to analog converter (DAC). This technique, usually referred to by the acronym SWIFT (for Stored Waveform Inverse Fourier Transform), is well known in the ICR community, but has never been discussed in full detail, and has so far been little used.

Due to the critical need for such technology presented by ICR cluster research we have implemented this SWIFT approach at the highest level we could achieve at the current stage of digital electronics. The bottom panel of Figure 3 shows an example of the resulting improvement in the rf excitation waveform. The panel shows the measured rf excitation spectrum produced by a 30 millisecond SWIFT waveform generated by a 14 bit DAC from a 128 kword inverse Fourier transform. Note this is not a computer simulation. The voltage waveform was generated by the SWIFT electronics, redigitized at 12 bits accuracy, and the resultant magnitude spectrum seen in Fig.3 was obtained from the computed Fourier transformation of this real data. The vast improvement in excitation control together with the far greater flexibility

and simplicity of operating with this fully computerized excitation waveform generation make this clearly the method of choice.

In the remaining portions of this section we provide details of our implementation of the electronics and computational aspects of the SWIFT technique. Uninterested readers may skip to section III with no loss of continuity.

SWIFT ELECTRONICS

Figure 4 presents a block diagram of the basic components of the SWIFT excitation waveform generator. It is designed around a high speed (10 MHz) 14 bit DAC fed from a commercially available 4 Mbyte 32bit VME buss dynamic random access memory (DRAM). Communication with our MicroVax II computer was performed through a standard CAMAC interface. Operation of the waveform generator is best explained by following a typical SWIFT waveform form its calculation in the computer to its final output as time varying voltage onto the ICR cell excitation plates.

SWIFT excitations are initially entered as rectangular blocks in frequency space. The inverse Fourier transform time domain signal is then calculated on a 40 Mflop array processor (CSPI MAP-4000), the resultant data being converted from 32 bit floating point to 16 bit integers before being sent over the CAMAC interface for storage in the 4 Mbyte VME memory of the waveform generator. Once stored, the data is accessed by pointers to its starting and ending addresses. In the current unit a single SWIFT waveform may be up to 2 million points long (extendable to 16 megapoints if necessary), but normally this extra memory is used to store a number of shorter waveforms for performing multiple ejections, and ultimately the final coherent excitation of the ICR transient for detection of the clusters left in the trap. This great versatility of having a number of stored waveforms in memory, each of which having no restrictions whatever in functional form, and being able to select them in any order entirely under computer control, is one of the major advantages of the SWIFT approach. Although the details of the electronics may seem complex, the effect of this full implementation of SWIFT

on the operation of the FT-ICR experiment is one of major conceptual and procedural simplification.

Before a particular stored waveform can be converted into an actual voltage signal the starting and ending addresses must be read in to dedicated 24 bit registers, the address generator is set to the starting address, and the internal clock is set to the desired conversion frequency (the rate at which the output voltage is updated to the next digital value). The master oscillator for this timing is a high accuracy 20 MHz temperature controlled crystal oscillator (TCXO) which feeds an 8 bit programmable frequency divider to produce the internal clock pulses. Once these parameters have been set by appropriate CAMAC commands, the SWIFT waveform generator simply waits for an external TTL synchronization pulse to be received at a BNC connection on the front panel.

Once triggered, data is read out of the main VME memory in 32 bit chunks and is temporarily stored in a 16 word long, 32 bit wide FIFO (first in first out) cache memory buffer as shown in the diagram of Fig. 4. This buffer functions as a data reservoir in case the main DRAM VME memory requires a refresh cycle during the readout. The 32 bit data is read out of the bottom of the FIFO at a constant rate of half of the internal clock frequency. It is sent to a 2:1 multiplexer where it is separated into two 16 bit words before being sent to the 14 bit DAC. This allows the DAC to run at twice the speed of the main memory. Since the DAC requires only 14 bits of data, the 2 remaining bits are available to generate timing pulses that can be used to synchronize external events.

The 5 volt peak-to-peak (pp) analog output voltage from the DAC is low-pass filtered by two commercial 1 MHz Bessel filters to remove any stray high frequency noise produced by the digital switching. The filtered SWIFT signal is then applied to the input of the rf power amplifier section shown in the bottom of Fig. 4. The phase splitter provides two versions of the SWIFT waveform 180^{o} out of phase for the two excitation plates of the ICR cell. The output voltage of each side is amplified to a maximum of 24 V pp. Note the pair of analog switches which ground the power amplifier inputs and isolate

them from the SWIFT output signal in order to minimize noise pickup when the ICR transient is being monitored.

SWIFT WAVEFORM CALCULATION

The SWIFT excitation waveforms in this implementation consist of a number of rectangular blocks in frequency space, each block being defined by a starting frequency F_1, a stopping frequency F_2, and an amplitude A. The desired waveform in frequency space , F(f), for this SWIFT block is then taken to be

$$F(f) = A \cdot R(x) \cdot P(x) \cdot \exp(it_o f) \cdot \exp(ikx^2), \qquad (1)$$

where f = the frequency (in Hz),

x = $(f-f_o)/W$,

W = the SWIFT block width (F_2-F_1),

f_o = the center frequency of the block $(F_1+W/2)$,

R(x) is a rectangle function centered at x=0:

$$R(x) = \begin{cases} 0.0 & \text{if } |x| > 0.5 \\ 0.5 & \text{if } |x| = 0.5 \\ 1.0 & \text{if } |x| < 0.5 \end{cases},$$

t_o and k are adjustable constants,

and P(x) = is an even polynomial in x.

First consider the function F(f) with the polynomial P(x)=1. The input function F(f) is then a square block of selected amplitude, width, and center frequency, multiplied by a polynomial and two complex phase factors. While these phase factors leave the rf power spectrum unchanged, they are critical in the practical generation of a real time-domain function, V(t), whose Fourier transform power spectrum in the frequency domain is F(f). The first complex phase factor is the most simple. Depending linearly on x, its effect is just to shift the inverse Fourier transform of F(f) along the positive time axis to center at $t=t_o$ so there is no appreciable intensity at negative time.

The second complex phase factor, however, is less trivial. It has been chosen to depend quadratically on x. The intent is to reduce the dynamic range of the digital-to-analog conversion necessary to faithfully generate the " t) waveform, so that its measured rf power spectrum actually turns out to be F(f). Without this phase term (equation (1) with k=0 and the polynomial P(x)=1) the real inverse Fourier transform[11], RIFT, of F(f) gives

$$\text{RIFT } F(f) = V(t) = V_o \cos(f_o(t-t_o)) \operatorname{sinc}(W(t-t_o)) \quad (2).$$

$$\text{where} \qquad V_o = W (2\pi A)^{1/2} .$$

Due to the sinc() function, this time domain waveform has the undesirable property of becoming very large and narrow at $t=t_o$ when the widtn of the frequency block, W, is substantial. With the 14 bit dynamic range of the DAC in the analog output stage of the SWIFT electronics (Fig. 4), and the 24 V pp limit of the power amplifiers that drive the excitation plates of the ICR cell it is not possible to generate a voltage waveform of sufficient accuracy. This difficulty was recognized by Marshall *et. al.* in their first presentation the SWIFT concept[9]. As they point out, the problem is due to the fact that all component frequencies of the waveform start out in phase at $t=t_o$.

Since the power of any particular frequency component is independent of its phase, in principle one can chose any phase factor one wants. As seen in equation (1) we have chosen a phase which depends quadratically on the frequency offset from the center frequency f_o of the SWIFT block. This is the same choice as suggested initially by Marshall[9,10]. Guan has recently argued that this quadratic phase factor is optimum for reducing the dynamic range of the SWIFT time domain waveform[12]. We find the best choice for the factor k is given by

$$k = W \cdot dt \cdot \pi/2 \qquad (2)$$

where as before W = the frequency width of the SWIFT block,
and dt = the time interval between points in V(t).

Figure 5 shows the relationship between the real and imaginary parts of F(f), as well as the phase, kx^2, for a hypothetical SWIFT block as a function of frequency. In order to make the phase relationships evident the value of k was reduced drastically for this figure. Note that in the center of the block the phase is zero and the imaginary part of F(f) is zero. The amplitudes of the real and imaginary parts begin to oscillate with increasing rapidly as the frequency approaches the block edges. As the quadratic phase parameter, k, is increased these oscillations occur more rapidly and the corresponding V(t) waveform becomes more evenly distributed in time. The value of k given above in equation (2) is chosen such that the largest phase change per point (which occurs at the edges of the block) is $\pi/2$, which is the maximum permitted by the Nyquist sampling theorem.

In spite of this quadratic phase modulation of the input frequency spectrum F(f) we have found it is still necessary to do a bit more to ensure that the V(t) waveform resulting from the inverse Fourier transform gives the desired square power spectrum. The polynomial function P(x) has been included in the definition of F(f) presented in equation (1) In order to achieve a flat, uniform power across the entire frequency block. Good results are obtained with

$$P(x) = 2.24\ x^2 + 3.35\ x^4 + 3.50\ x^6 + 3.75\ x^8.$$

Figure 6 shows the measured magnitude spectrum of a 128k point SWIFT waveform generated by the electronics of Fig. 2 from the calculated RIFT of a 64kword F(f) block generated by setting F_1 = 10.0 kHz, F_2 = 15.0 kHz, and evaluating equation (1) at all frequencies between 0 and 2.5 MHz at successive intervals of 38.14697 Hz. The internal clock of the SWIFT waveform generator was set to 5 MHz, resulting in a V(t) waveform duration of 26.2 milliseconds. This V(t) waveform was digitized with 12 bit accuracy for a 64 kword record length and then Fourier transformed to generate the rf magnitude spectrum shown in Fig 6.

As is evident in the top panel of Fig. 6 the generated waveform has a magnitude spectrum which is quite close to the desired square block. The only remaining problem is a bit of oscillation near the edges of the block,

including a bit of "leakage" of rf power to frequencies slightly outside of the block. This is predominantly due to the fact that the SWIFT time domain waveform was of finite length. This effect may be moderated by multiplying the V(t) waveform with a Hamming window apodization function[10,13], W_H:

$$W_H(t) = 0.54 - 0.46\cos(2\pi t/(N \cdot dt));$$

where t = time in seconds,
dt = the time interval between points
N = the total number of points in the V(t) waveform.

It is clear in the lower panel of Fig. 6 that this apodization has succeed well in removing the "leakage" and most of the oscillations near the edges.

For most of critical applications encountered in cluster studies the relevant question is how cleanly one can eject unwanted clusters from either side of a particular cluster isotopic variant, or group of isotopes. In this case two SWIFT blocks are defined, one on either side of the desired clusters to be preserved. Their inverse Fourier transforms are calculated and then added together. Figure 7 shows the measured result of such a twin SWIFT waveform as generated by the new apparatus. Here several different choices of the apodization function[12] are compared. It is evident that the best resolution in between the two blocks is obtained without any apodization at all. However, since the Hamming window function is nearly as good in resolution and is far better in terms of the smoothness of the rf magnitude spectrum and the absence of leakage, we have adopted it's use in all our subsequent work.

Figure 8 shows one example of the use of this new SWIFT apparatus to select individual isotopic mass peaks from germanium clusters in the cluster FT-ICR apparatus. We believe the electronic aspects of this approach are now worked out with sufficient care that the degree of perfection in selective excitation and ejection of clusters is limited only by dephasing processes in the ICR cell itself.

III. RESULTS

Figure 9 shows the FT-ICR mass spectrum of a typical distribution of silicon cluster ions injected and thermalized in the ICR trap. In the top spectrum the many isotopic variants are evident for each cluster size. The bottom mass spectrum shows the contents of the ICR cell after a SWIFT excitation which selectively ejected all but the most intense isotopic peaks for each cluster size in the cell. Note also that the baseline has been cleaned up considerably. Figure 10 shows this well-swept bare cluster distribution again and the mass spectrum after exposure to $4x10^{-7}$ torr NH_3 at 300K for 4 seconds. Due to the SWIFT selection of a narrow isotopic distribution, the $Si_x(NH_3)_y^+$ reaction products are quite clearly resolved. They have been labelled in the figure in the form "xA_y". Note that the sharp variation in reactivity towards chemisorption of ammonia reported briefly in our original paper is now quite vivid. Under these conditions some bare clusters such as Si_{44}^+ and Si_{46}^+ have nearly vanished, most of them being seen now in the mass spectrum with one or two NH_3 molecules chemisorbed in some form on their surface. On the other hand Si_{45}^+ has been effectively inert during this time.

In our original paper[1] it was not clear whether or not there had been some hydrogen loss during the chemisorption. The complexity of the many isotopic peaks for each cluster prevented a clean measurement of the mass shift for each chemisorption step. In these new experiments, however, it is now clear that each NH_3 chemisorption step proceeds with a mass shift of 17 amu -- there is no hydrogen loss. This does not necessarily mean that the chemisorption is not dissociative, however.

Many experiments such as the one shown in Fig. 10 were done for all Si_x^+ clusters from x=5 to 65 atoms. In all cases basically the same surface chemistry was observed: chemisorption without hydrogen loss. The principle results are summarized in Figure 11 which presents the estimated reaction rate constant for the chemisorption of the first ammonia on the bare silicon clusters as a function of cluster size. In order to deduce these rates a series of experiments were done with successively longer exposure times to the ammonia carrier gas. All were performed at the same total pressure ($1x10^{-5}$

torr), with mixtures of 1% NH_3 in argon for the more reactive clusters and 10% NH_3 in argon for the least reactive. The intensity of the mass peaks due to the unreacted cluster for each particular size was measured and ratioed to the integrated intensity of the bare cluster and all its reaction products. The reaction rates plotted in Fig. 11 are least squares estimations of the best straight line fit to a plot of the log of the measured concentration ratios versus the reaction time.

Replicate experiments were performed and the resulting precision estimates of the rate values are represented by the error bars plotted in Fig. 11. We believe the errors in relative reactivities are well represented by these error bars, but caution the reader about the absolute scale. The effective pressure of NH_3 in the ICR cell during the reactions was estimated from ionization gauge readings in the vacuum manifold just above the turbopump at the end to the ICR apparatus shown in Fig. 1. The estimation involved calculated conductances and may have been off by as much as a factor of 10. The reaction rates plotted in Fig. 11 for the most reactive clusters such as Si_{43}^+ and Si_{36}^+ are all about the same. For comparison the $Si_x^+ + NH_3$ collision rate calculated by the ADO theory of Bowers and Su[14] is also plotted in Fig. 11. We would not be surprised to find that our pressure calibration was off sufficiently that these two rates were really the same, implying that the most reactive cluster react effectively on every collision. The reaction rates of the most reactive clusters would therefore be nearly equal for a very simple reason: they just can't react any faster.

Figure 12 gives an example of some of the data used to generate the reaction rate estimates. The top panel shows the initial cluster distribution in 19-21 atom size range after a SWIFT ejection. Note that there is a small amount of reaction of Si_{20}^+ here to form the $Si_{20}(NH_3)^+$ reaction product even though no NH_3 reactant was added. This was due to a small residual pressure in the cell due to outgassing of ammonia from the ICR cell surfaces from previous reaction experiments. The second panel show the result of an identical experiment except that the clusters were exposed for 10 seconds to a 1% NH_3 mixture in an argon buffer gas at a total pressure of 1×10^{-5} torr. The 20th cluster has reacted extensively, while only a small amount of reaction is evident for 19 and 21. The subsequent two panels show the result of repeating

the experiment with 20 and 30 second exposure times to the same reaction mixture.

Figure 13 plots the results of many reaction studies such as that shown in Fig. 12 for silicon clusters 19-21 as a function of exposure time to the ammonia/argon mixture. Note that while the reaction data for Si_{19}^+ is well described by a straight line, corresponding to a single reaction rate, Si_{20}^+ and Si_{21}^+ have a more complicated reaction behavior. In the case of Si_{21}^+ there appear to be two distinct forms of the cluster: one that reacts fairly rapidly, and one that is fairly inert. This fact is reflected in the reaction rate estimates plotted in Figure 11 where Si_{21}^+ has two plotted rates. Similarly, there are two rate values plotted for Si_{20}^+ and quite a number of other clusters in the 6-65 size range. This evidence for multiple structural forms was common in the 20-25 atom size range, and for nearly all clusters above 49 atoms in size.

When considering this, remember that the smaller clusters were produced for these experiments without any ArF excimer laser reionization step. The ArF laser was only used for clusters larger than Si_{25}^+. Subsequent experiments have shown that laser excitation efficiently anneals these silicon clusters[5]. Inadvertently in these experiments the ArF reionization laser provided some annealing. We believe this explains the apparent absence of multiple structural forms in the 26-49 atom size range. For clusters 19 atoms and smaller, direct formation in the laser vaporization source appeared to anneal the clusters well enough even without an extra laser excitation such that all the reaction data appeared to fit well to a single rate. Above 19 atoms without the ArF reionization step, and above 49 atoms even with this step, adequate annealing apparently was not achieved in the results reported here.

The 100/1 argon/ammonia reaction mixture used to record the data of Figure 12 was intended to check the dependence of the measured apparent reaction rate on total pressure. In this cluster ICR apparatus the maximum number of collisions with a neutral gas that can be tolerated before unacceptable signal loss occurs due to diffusion of the cluster ions from the cell is roughly 50,000. As a consequence, the surface chemistry can only be probed at relatively low total pressure. There is always a concern therefore

that the apparent reaction rate is much too slow due to the fact that the trapped cluster ion immediately after reaction is hot as a result of the exothermicity of the reaction, and the chemisorbed molecule may desorb before it can be detected.

To the extent this desorption problem effects the reaction rates they should be sensitive to the total gas pressure used. We verified this fact by measuring the apparent reaction rate of ethylene with Si_{10}^+, which was chosen since it is a fairly small cluster where this effect may be important, and since Jarrold and coworkers[15] had published results of similar experiments at higher pressures in a tandem quadrupole experiment. As expected, we observed a reaction rate several orders of magnitude lower than measured by the Jarrold group, and found this apparent low reaction rate increased linearly with ethylene and/or argon pressure in the ICR cell at a rate consistent with that reported by Jarrold *et. al.*[15] (we also observed evidence for two forms of Si_{10}^+). An identical experiment performed in the ICR cell with ammonia showed the apparent rate to increase only be a factor of 2-3 when the net pressure was increased by a factor of 10. Therefore we believe that the Si_x^+ + ammonia reaction rate data presented in Figure 11 is somewhat affected by desorption in the small size range. However, for the very reactive clusters in the size region around Si^+_{43} the apparent reaction rate was insensitive to argon pressure in the range of 10^{-7} to 10^{-5} torr.

NEGATIVE SILICON CLUSTER REACTIVITY

Negative silicon cluster ions in the mass range from 20-50 atoms in size were also examined for reactivity toward NH_3. All were found to be far less reactive than the corresponding positive clusters, requiring such a large number of collisions that most cluster ions migrated out of the ICR cell before a significant reaction product distribution was evident. As shown in Fig. 11, we concentrated on the size region between 39 and 50 atoms. These clusters were made in the same fashion as the positive clusters, using an ArF reionizing laser as the clusters began their expansion. Of all the clusters studied in this region, only Si_{43}^- reacted at a sufficient rate that less than 10% remained unreacted at the longest possible exposure times. As plotted in

Fig. 11, some of the other clusters were observed to react as well, but we were unable to observe this reaction long enough to be sure the measured rate was representative of the bulk of the clusters of that particular size in the cell.

IV. DISCUSSION

The experiments reported here have been under consideration for approximately one year as we have made careful checks, repeated the reaction experiments under different conditions, and even gone to a completely new source and injection scheme[7]. Partially in response to an early survey of the results we were obtaining[3], Jarrold's group has published extensively on silicon cluster reactivity experiments they have performed with a tandem quadrupole instrument over this period[8,15-17], and some rather distinct differences have emerged between our two groups. As we stated in our original communication three years ago[1], and now reconfirm with the data of this paper as summarized in Fig. 11, we find clear evidence for special reactivity behavior of certain clusters, particularly those with 21, 25, 33, 39, and 45 atoms. Jarrold's group, on the other hand, has found little difference between these and any other cluster in the 20-50 atom size range.

In a recent short paper based on the new version of this ICR apparatus it was demonstrated that annealing is critical to the observation of these special size effects on the reactivity[5]. Operating with silicon cluster ions prepared in a pulsed source that directly injected the supersonic cluster beam into the ICR cell, it was unnecessary to use the ArF excimer laser for the "reionization" needed for the study of clusters larger than 25 atoms as reported here. While some differences in the reactivity toward ammonia were evident when the clusters were studied right after injection, the difference became vivid after the clusters were laser annealed: Si_{45}^+ became completely inert while Si_{42}^+ became even more reactive.

Other experiments done a month earlier on this new apparatus with ethylene chemisorption[6] had shown that this reagent also senses a major difference between these clusters. In the region between 36 and 50 atoms the

reaction pattern of the positive silicon clusters toward ethylene was much like that shown here for ammonia, except without intentional laser annealing as we now do routinely[5,18] (or unintentional laser annealing with an ArF laser as done in the original ammonia experiments[1] and those reported here) there was a substantial component of fairly reactive isomeric forms present in the ICR cell even for the most "magic" clusters Si_{39}^+ and Si_{45}^+. It was demonstrated that even without annealing, these less well-formed geometrical isomers of the clusters like 39 and 45 could be largely reacted away.

We believe, therefore, that the majority of the differences between the results of Ray and Jarrold compared to our own is due to annealing. In the original experiments and these somewhat more refined measurements reported here, we fortuitously managed to generate a population of structural isomers that was dominated by the lowest energy, best "reconstructed" geometrical forms possible, particularly in the 25-48 atom size range. For reasons that are not yet entirely clear, the cluster source used by Ray and Jarrold is not nearly so effective. Anderson et. al. have argued that the critical difference may be in the time scale for the cluster formation, or the time scale for their subsequent cooling[6].

Ray and Jarrold have also considered the possibility that we may be measuring two entirely different chemical processes (dissociative chemisorption in the case of these low pressure ICR experiments, molecular chemisorption in their case of much higher pressure, much shorter time scale reactions). We find the arguments they put up against this explanation to be compelling -- particularly since we are measuring reaction rates for our most reactive clusters (eg. Si_{43}^+) which seem to saturate at a level within an order of magnitude of theirs (and may be equal to theirs when our pressure calibration is improved), and since we see no effect of pressure on the apparent reaction rate. For clusters in the 10-20 size range where we expect our data is slightly affected by desorption there is still considerable agreement between the two groups. Both groups find clusters 11, 13, and 19 to be local minima in the reactivity pattern. Above 19 atoms without ArF excitation and its corresponding annealing effects we find extensive evidence of multiple structures whose peak reaction rates are all about the same, and close to the collision rate.

It is not clear yet whether any of this surface chemistry is dissociative chemisorption of the sort that is known to occur on bulk Si surfaces such as the 7x7 reconstruction of Si(111)[19]. The only clear evidence we have observed for dissociation was found in reactions of Si_{10}^+ with very large amounts of NH_3 where mass peaks corresponding to successive losses of H_2 were seen on the products that had chemisorbed more than 3 ammonia molecules. This evidence was quite clear, but we have yet not seen it reproduced for any larger cluster, and it may have been due to a secondary reaction of molecularly adsorbed NH_3 groups after the effective cluster temperature had risen from multiple chemisorptions. This issue deserves extensive scrutiny with laser excitation and isotopic tracers in future ICR experiments.

Further evidence that what is being dealt with here is the existence of special structures for silicon clusters is found in the negative ion experiments reported above. Although we were unable to push the reactions far enough to gain a clear picture, the fact that Si_{43} is the most reactive cluster of both the positive and negative cluster distributions is quite a coincidence. Interestingly, positive germanium clusters present much the same result[7]. Here none of the clusters react with NH_3 under our conditions, but with NO the most reactive cluster is, once again, Si_{43}. Photofragmentation results obtained in some of the very earliest semiconductor cluster experiments in this group[20] gave evidence that the structure of silicon and germanium clusters may be much the same. These new reactivity results now lend support to this hypothesis. It may be that the structural packing arrangements that most efficiently tie up dangling bonds for any particular cluster size are basically the same for all the semiconductors which are 4-coordinated, and adopt the diamond lattice in the bulk phase. This concept may even extend out of Group IV to GaAs clusters, for example[21].

PROPOSALS FOR SILICON CLUSTER STRUCTURE

If one grants that special well-formed clusters of silicon appear in these experiments, then there is good cause for considerable effort to try to imagine what these structures may be, to design theoretical calculations to

predict their properties, and to design experiments to test these theories. While we do not yet have a method for direct structural determination, it is nice to know that at least in some special cases there is one structure that is best -- a structure that dominates in the limit of good annealing, and one that can be made reliably for a wide range of cluster surface experiments. Until some direct probe is developed (eg. the gas phase cluster equivalent of STM for the 7x7 (111) surface of bulk silicon[19,22]) we will have to deal with educated guesses followed by detailed experiments to choose between alternatives.

A substantial amount of this educated guessing has been going on already[23-35]. For silicon the 10th cluster attracted the most interest early on. Initial results showing it to be specially abundant in the cluster mass distribution[23] led initially to the suggestion that it was simply a piece of the bulk diamond structure -- an adamantane cage without the hydrogens. Early calculations of Raghavachari[24] showed that a much better structure is formed by distorting this adamantane cage by elongating it along its four 3-fold vertices so that its 2-fold vertices could begin to participate in more than 2 bonds. The result is a sort of "pyramid with elbows" which is usually described the literature as a tetacapped octahedron. Often this structure is taken as evidence that the small clusters are reminiscent of the high pressure metallic phases of silicon, as distinct from the semiconducting diamond lattice[28]. In view of the substantial HOMO-LUMO gap in this cluster[36], we prefer to think of it as a covalently bonded piece of the bulk diamond lattice which has undergone a mild relaxation in order to patch up the surface dangling bonds as best as possible. Ballone and coworkers[25] have suggested another structure for Si_{10} based on local density calculations which appears to be just as stable[27]. It is a tetacapped trigonal prism -- a polyhedral structure which is less readily related to the bulk lattice. Even so we suspect the bonding in such structures is still best thought of in covalent terms. Patterson and Messmer[34,35] have discussed at length the virtues of thinking about these small silicon clusters with basically the same covalent bonding concepts used for small silicon-containing molecules and the bulk covalent lattice.

For clusters larger than 10 atoms the number of conceivable structures grows rapidly. While in the size range from 10-20 the reasonable structures are all either polyhedra or capped polyhedra which are fairly easy to systematize and consider one by one, above 20 the possible structures rapidly become far more numerous and complex. As yet the simulated annealing approach used first on silicon by Ballone *et. al.*[25] has not been implemented on a sufficiently fast computational engine to be able to handle clusters the size of Si_{45}. Although such a calculation may be possible within a few years, if may be possible to guess the right answer in advance.

One clue may be provided by the fact that in Fig. 11 most of the clusters do react rather readily. It is the unreactive clusters that are special. Somehow clusters of these special sizes have apparently be able to restructure themselves so that what is a fairly easiiy achieved reactive site has been avoided all around the surface of the cluster. Avoiding active sites is apparently difficult, so it is perhaps wise to search among high symmetry structures where a few particularly good ways of avoiding an active site have been successfully replicated around the entire surface.

Another clue is the fact that these fairly large clusters tend to fragment by fission, releasing units in the 6-11 atom size range. The fact that germanium clusters fragment the same way suggests this is a property of the bonding[20]. It suggests that the large clusters have natural cleavage planes such as the (111) plane of bulk silicon[20,23].

As we pointed out in our original short communication[1] about special behavior of such clusters as Si_{39}^+, clusters in this 30-50 atom size range are large enough to have at least five tetrahedrally bonded silicon atoms with all four valences satisfied. A beautiful example of such a structure was proposed by Kaxiras[32,33] for the case of Si_{45}. As seen in the top panel of Figure 45, this structure has a central tetrahedral atom whose bonding structure is very much like that found in the bulk diamond lattice. Its high symmetry and easy cleavage to split off a 6- or 10-membered fragment make it nicely in accord with the two clues.

FILLED FULLERENES

There is an interesting connection to carbon here. Note that the Kaxiras Si_{45} structure in top panel of Fig. 45 consists of a central atom surrounded by a network of 5- and 6-membered rings. There are 4 groups of 3 pentagonal rings arranged at the vertices of a tetrahedron, and 4 groups of 3 hexagonal rings at whose common vertex is a point of attachment to the central silicon atom. If one cuts the connections to the central atom and smooths the cluster out to a spheroidal shape, it is evident that this is a 44 atom fullerene similar to those proposed to account for the specially inert even-numbered distributions found for carbon clusters[37]. So the Kaxiras Si_{45} structure may be thought of as a sort of "filled fullerene" which has tied up the dangling bonds of the surface as best as possible through interconnected 5- and 6-membered rings, and connected on the inside to a fully 4-coordinated inside atom.

These fullerene structures consist of 12 5-membered rings, and any number of 6-membered rings (except 1). For any particular fullerene cage there are generally many isomeric forms given by the different ways of arranging the pentagons. Starting at Si_{21}^+ we have found a set of filled fullerene structures which are in accord with the special numbers 21, 25, 33, 39, and 45. While these structures seem appealing, we have as yet no strong arguments that they should be the best. However, one interesting aspect is that this filled fullerene model does predict that somewhere between 45 and 54 atoms the size of the fullerene cage becomes too large to connect to just a single internal atom without excessive strain. The model then predicts that the odd-numbered sequence seen in the 21-45 atom range would switch to a sequence of even-numbered special clusters having two internal atoms. There is a hint of this in the reactivity pattern of Fig. 11 seen for the cluster Si_{54}^+, but this is beyond the range of effective annealing in these experiments. Future work with laser annealed clusters will test this prediction in detail.

There are, of course, many other structures possible for these large clusters. The bottom panel of Fig. 14 shows an alternative for Si_{45}^+ proposed by Patterson and Messmer[34]. This structure is highly symmetric and is also a filled polyhedron, except in this case polyhedron includes 6 four-membered

rings. They have proposed a series of similar structures to explain the 21, 25, 33, 39, 45 sequence. Their proposed structure[34] for Si_{33}^+ is the same as one proposed by Kaxiras[33]. It is a filled 28 atom fullerene with one atom on the inside to make Si_{29}. The proposed 33 atom structure is formed by capping each of the 4 "adatom sites" on the surface of this cluster much as the corresponding sites are capped on the 7x7 (111) surface of bulk silicon.

It will be interesting to see the interplay between theory and experiment over the next few years as these special structures are elaborated and tested.

ACKNOWLEDGEMENT

We thank Martin Jarrold for stimulating discussion and communication of his results prior to publication, and Fellipe Chibante and LiHong Wang for extensive help during conversion of the FT-ICR apparatus to turbopumped operation. This research on semiconductor clusters was funded in part by the Office of Naval Research, and the Robert A. Welch foundation, using portions of a cluster ICR apparatus funded for bare metal cluster research by the US Department of Energy, Division of Chemical Sciences, for gallium arsenide cluster research by the US Army Research Office, and for studies of chemisorbed species on clusters by the National Science Foundation.

REFERENCES

1) J.L. Elkind, J. M. Alford, F. D. Weiss, R. T. Laaksonen, and R. E. Smalley, J. Chem. Phys. 87, 2397 (1987).

2. J. M. Alford, P. E. Williams, d. J. Trevor, and R. E. Smalley, Int. J. Mass Spectrom. Ion Phys. **72**, 33 (1986).

3). J. M. Alford and R. E. Smalley, Mat. Res. Soc. Symp. Proc. 131, 3 (1989).

4. J. L . Elkind, F. D. Weiss, J. M. Alford, R. T. Laaksonen, and R. E. Smalley, J. Chem. Phys. 88 5215 (1988).

5. S. Maruyama, L. R. Anderson, and R. E. Smalley, J. Chem. Phys. in press.

6. L. R. Anderson, S. Maruyama, and R. E. Smalley, Chem. Phys. Lett. submitted.

7. S. Maruyama, L. R. Anderson, and R. E. Smalley, Rev. Sci. Instrum., submitted.

8. U. Ray, and M. F. Jarrold,"Interaction fo Silicon Cluster Ions with Ammonia: The kinetics" J. Chem. Phys. in press.

9. A. G. Marshall, T. C. L. Wang, and T. L. Ricca, J. Am. Chem. Soc. 107, 7893 (1985).

10. A. G. Marshall and F. R. Verdun, Fourier Transforms in NMR, Optical, and Mass Spectrometry (Elsevier, Amsterdam, 1990).

11. see for example W. H. Press, B. P. Flannery, S. A. Teukolsky, and W. T. Vetterling, Numerical Recipies in C (Cambridge University Press, Cambridge, 1988) pp 398-425.

12. S. Guan, J. Chem. Phys. 91 775 (1989).

13. F. J. Harris, Proceedings of the IEEE, 66 1 (1978).

14. a) T. Su and M. T. Bowers, J. Chem. Phys. **58**, 3027 (1973); b) T. Su and M. T. Bowers, in "Gas Phase Ion Chemistry", Vol 1, M. T. Bowers, editor (Academic Press, New York, 1979).

15. M. F. Jarrold, J. E. Bower, and K. M. Creegan, J. Chem. Phys. 90, 3615 (1989).

16. K. M. Creegan and M. F. Jarrold, J. Am. Chem. Soc. 112, 3768 (1990).

17. M. F. Jarrold, U. Ray, and K. M. Creegan, J. Chem. Phys., in press (1990).

18. Current experiments with trimethylamine also show the same reaction pattern with silicon clusters as reported here in the 36-50 size range once the clusters have been annealed with pulses from XeCl laser -- L.P.F. Chibante, M. G. Simmons, and L. Anderson , work in progress.

19. Ph. Avouris, J. Phys. Chem. 94, 2246 (1990).

20. Q. L. Zhang, Y. Liu, R. F. Curl, F. K. Tittle, and R. E. Smalley, J. Chem. Phys. 88, 1670 (1988).

21. C. Jin, K. J. Taylor, J. Conceicao, and R. E. Smalley, Chem. Phys. Lett., submitted.

22. G. Binnig, and H. Rohrer Rev. Mod. Phys. 59 615 (1987).

23. L. A. Bloomfield, R. R. Freeman, and W. L. Brown, Phys. Rev. Lett. 54, 2246 (1985).

24. K. Raghavachari, Z. Phys. D - Atoms, Molecules, and Clusters, 12, 61 (1989).

25. P. Ballone, W. Andreoni, R. Car, and M. Parrinello, Phys. Rev. Lett. 60, 271 (1988).

26. D. Tomanek and M. A. Schluter, Phys. Rev. B36 1208, (1987).

27. K. Raghavachari and C. M. Rohlfing, J. Chem. Phys. 89, 2219 (1989).

28. J. R. Chelikowsky and J. C. Phillips, Phys. Rev. Lett. 63 1653 (1989).

29. S. Saito, S. Ohnishi, C. Satoko, and S. Sugano, Z. Phys. D - Atoms, Molecules, and Clusters, 14, 237 (1989).

30. J. C. Phillips, J.Chem. Phys. 88, 2090 (1988).

31. D. A. Jelski, Z. C. Wu, T. F. George, Chem. Phys. Lett. 150, 447 (1988).

32. E. Kaxiras, Chem. Phys. Lett. 163, 323 (1989).

33. E. Kaxiras, Phys. Rev. Lett. 64, 551 (1990).

34. C. H. Patterson and R. P. Messmer, Phys. Rev. B in press, (1990);

35. C. H. Patterson and R.P. Messmer, Phys. Rev. Lett. submitted.

36. O. Cheshnovsky, S. H. Yang, C. L. Pettiette, M. J. Craycraft, Y. Liu, and R. E. Smalley, Chem. Phys. Lett. 138, 119 (1987).

37. R. F. Curl and R. E. Smalley, Science 242 1017 (1988).

FIGURE CAPTIONS

Figure 1. Schematic of the supersonic cluster beam FT-ICR apparatus.

Figure 2. Schematic drawing of the supersonic ion beam extraction, injection, and trapping electrodes of the cluster FT-ICR apparatus.

Figure 3. Comparison of the measured Fourier transform magnitude spectrum of an rf frequency-swept excitation scan (A) with a "SWIFT" excitation set for the same specified range of 10.0 to 15.0 kHz.

Figure 4. Diagram of functional units of the SWIFT stored waveform electronics for selective excitation and/or ejection of cluster ions trapped in the ICR cell.

Figure 5. Imaginary (top), real (middle), and phase (bottom) components of the quadratic phase shifted function F(f) whose inverse Fourier transform is used to produce a SWIFT excitation waveform.

Figure 6. Comparison of the measured Fourier transform magnitude spectrum of SWIFT excitation waveforms generated either without apodization (top) or with a Hamming window apodization (bottom).

Figure 7. Comparison of various apodization functions illustrating the loss of resolution of the ejection notch versus the reduction in rf power "leakage".

Figure 8. Demonstration of the use of SWIFT to select a single isotopic peak out of the broad isotopomer distributions for Ge_{11}^+ and Ge_{12}^+. A triple block SWIFT excitation was used as outlined in the top panel.

Figure 9. FT-ICR mass spectrum of silicon cluster positive ions in the range from 44 to 54 atoms in size as they appear after injection (top), and as they appear after a SWIFT ejection was performed to select a narrow range of cluster masses for further study.

Figure 10. Ammonia chemisorption study of silicon cluster ions in the FT-ICR. The top panel shows the clusters prior to reaction, with most of the isotopic complexity removed by a SWIFT ejection. The bottom panel shows the result of exposure to ammonia for 4 seconds at a pressure of $4x10^{-7}$ torr. The chemisorption products are of the form $Si_x(NH_3)_y$; they are labeled "xA_y".

Figure 11. Estimated reaction rates for chemisorption of the first ammonia on silicon cluster ions as a function of cluster size. All measurements on the positive cluster ions were performed with argon/NH_3 mixtures at a total pressure of $1x10^{-5}$ torr in the ICR cell. The negative clusters were measured with pure NH_3 at $1x10^{-4}$ torr. Note that due to inadequate annealing some clusters in the 20-25 size range and those larger than 48 atoms showed evidence for at least two structural forms with different reaction rates.

Figure 12. Reaction study of Si^+_{19-21} in the ICR trap as a function of exposure time to a mixture of ammonia and argon. The successive ammonia chemisorption adducts, $Si_x(NH_3)_y$ are labeled in the form "xA_y". The small peaks corresponding to $Si_{20}NH_3^+$ in the top mass spectrum resulted from reactions with a small residual background pressure of NH_3 in the apparatus.

Figure 13. Log plot of the relative Si^+_{19-21} cluster signal as a function of reaction time in the FT-ICR trap. The curves are the results of least squares fits of the data to either a single exponential function (for Si_{19}^+), or a bi-exponential.

Figure 14. Two proposals for the structure of the particularly unreactive cluster Si_{45}^+: the top structure is the proposal of Kaxiras (ref.), the bottom is due to Patterson and Messmer (ref.).

Figure 15. Scheme for generating a Si_{33}^+ structure by adding four cap atoms to a tetrahedral "filled fullerene" Si_{29}^+.

Figure 1

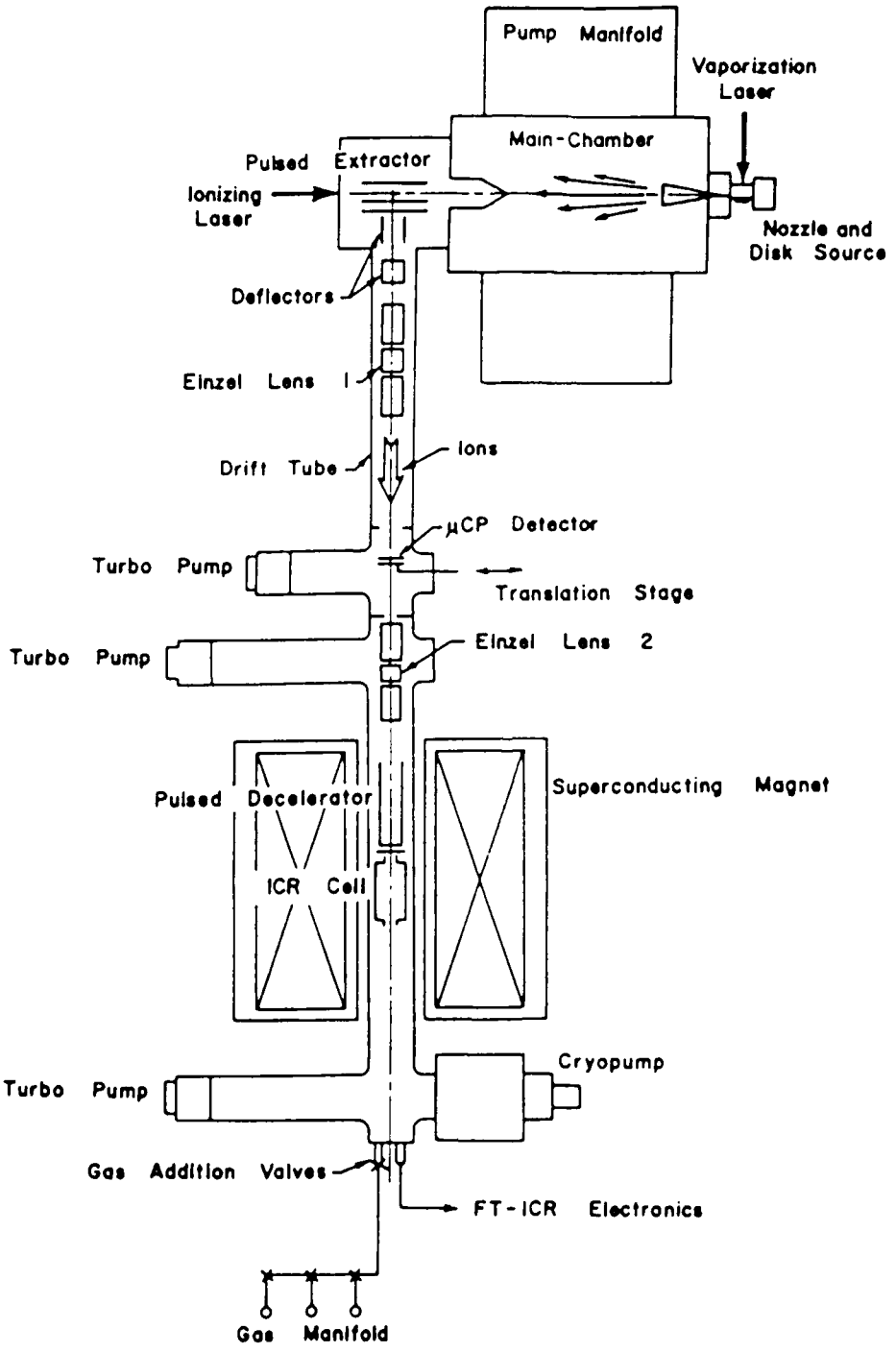
Pump Manifold
Vaporization Laser
Main-Chamber
Pulsed Ionizing Laser
Extractor
Nozzle and Disk Source
Deflectors
Einzel Lens 1
Drift Tube
Ions
μCP Detector
Turbo Pump
Translation Stage
Turbo Pump
Einzel Lens 2
Pulsed Decelerator
ICR Cell
Superconducting Magnet
Cryopump
Turbo Pump
Gas Addition Valves
FT-ICR Electronics
Gas Manifold

Figure 2

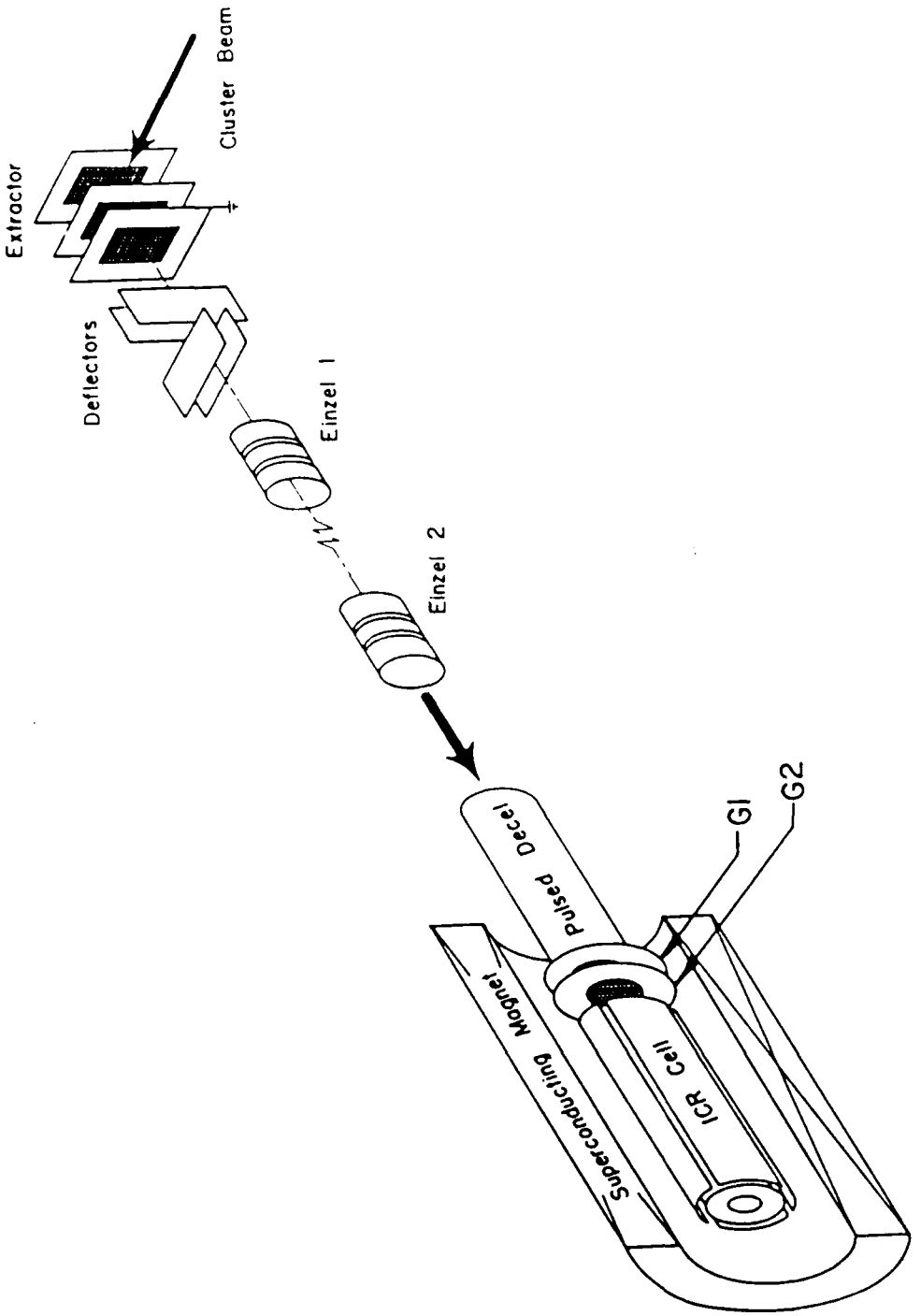
Cluster Beam
Extractor
Deflectors
Einzel 1
Einzel 2
Pulsed Decel
G1
G2
Superconducting Magnet
ICR Cell

Figure 3

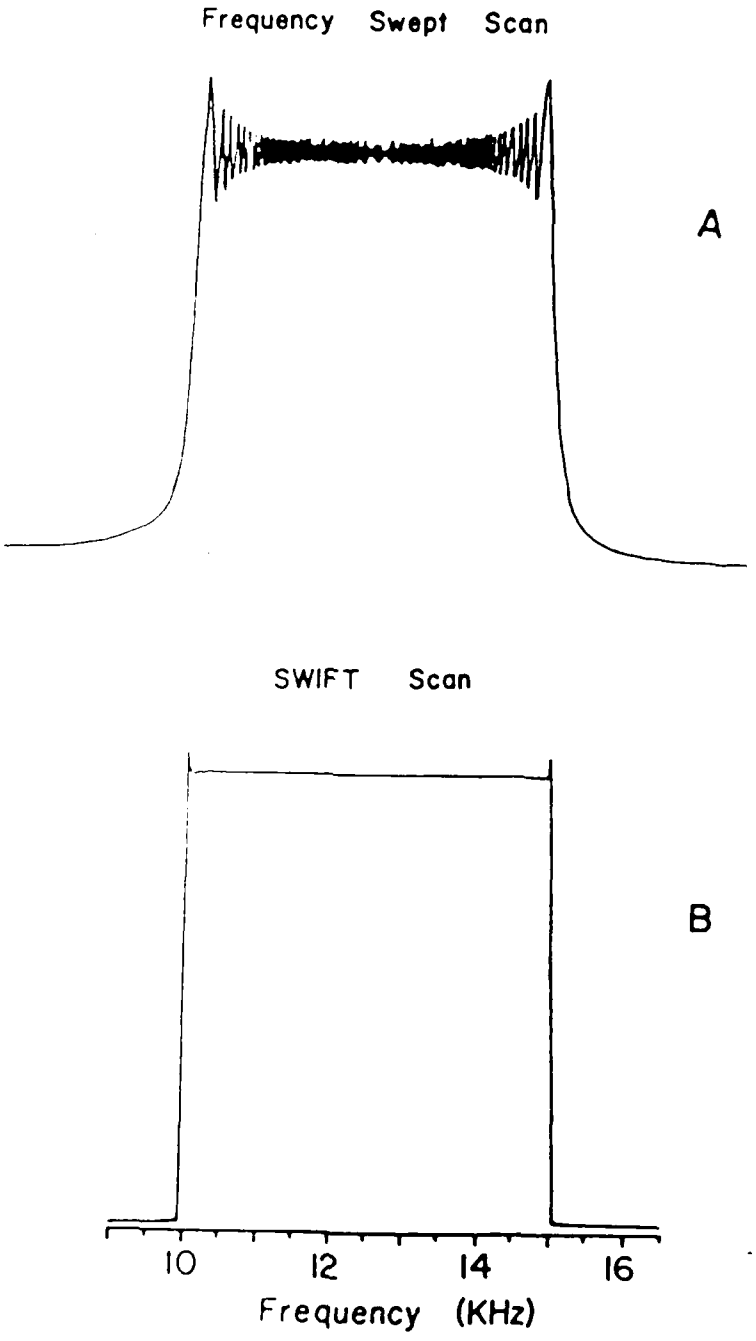

Figure 4

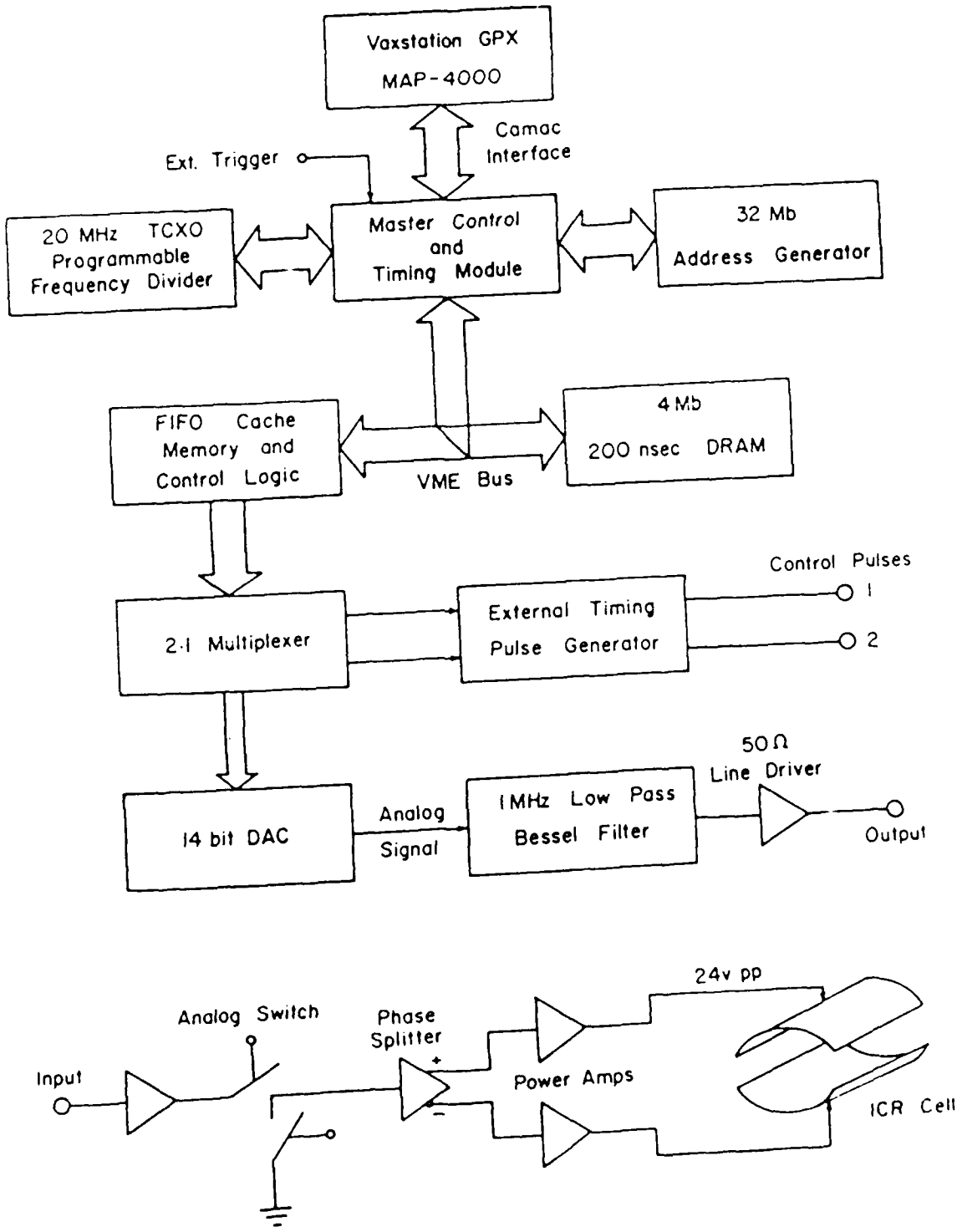
Vaxstation GPX
MAP-4000
Camac
Interface
Ext. Trigger
20 MHz TCXO
Programmable
Frequency Divider
Master Control
and
Timing Module
32 Mb
Address Generator
FIFO Cache
Memory and
Control Logic
VME Bus
4 Mb
200 nsec DRAM
Control Pulses
1
2
2-1 Multiplexer
External Timing
Pulse Generator
50 Ω
Line Driver
14 bit DAC
Analog
Signal
1 MHz Low Pass
Bessel Filter
Output
24v pp
Analog Switch
Phase
Splitter
Input
Power Amps
ICR Cell

Figure 5

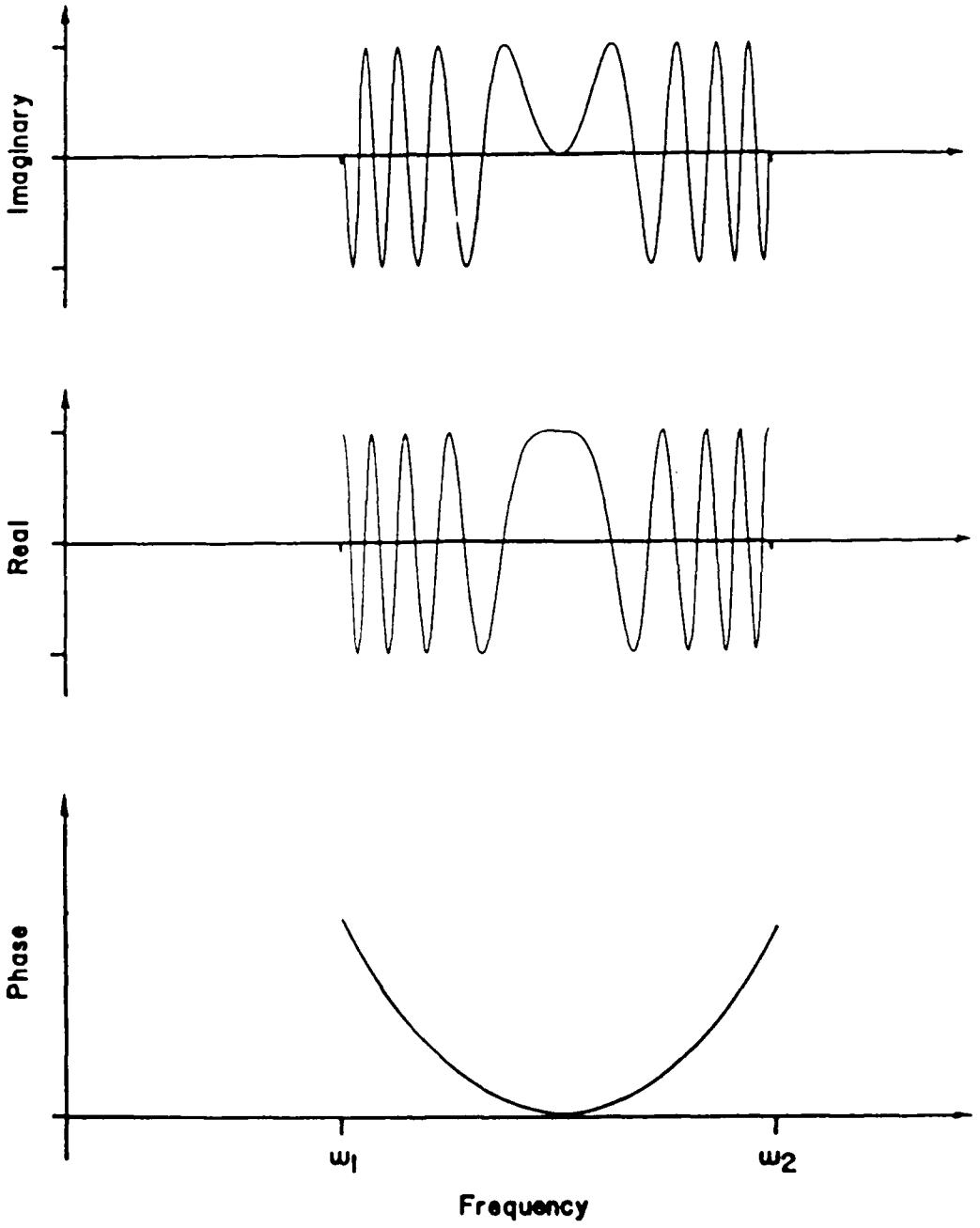

Figure 6

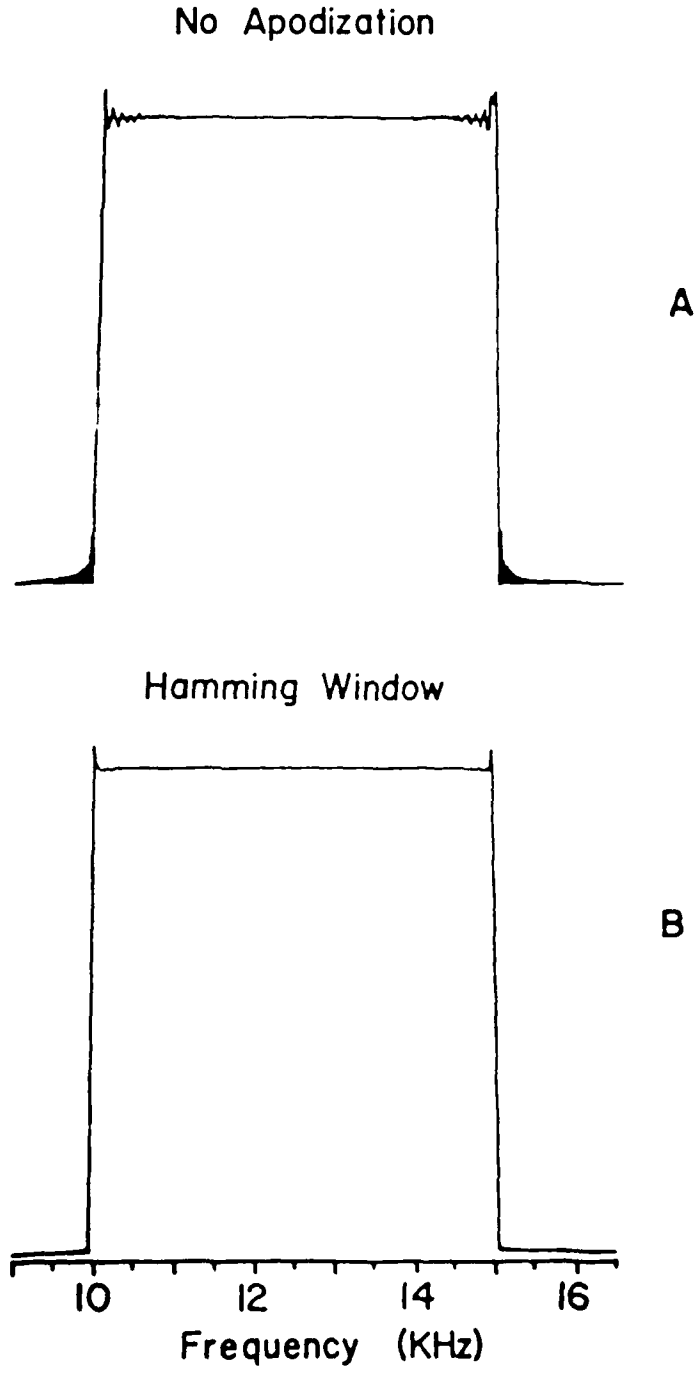

Figure 7

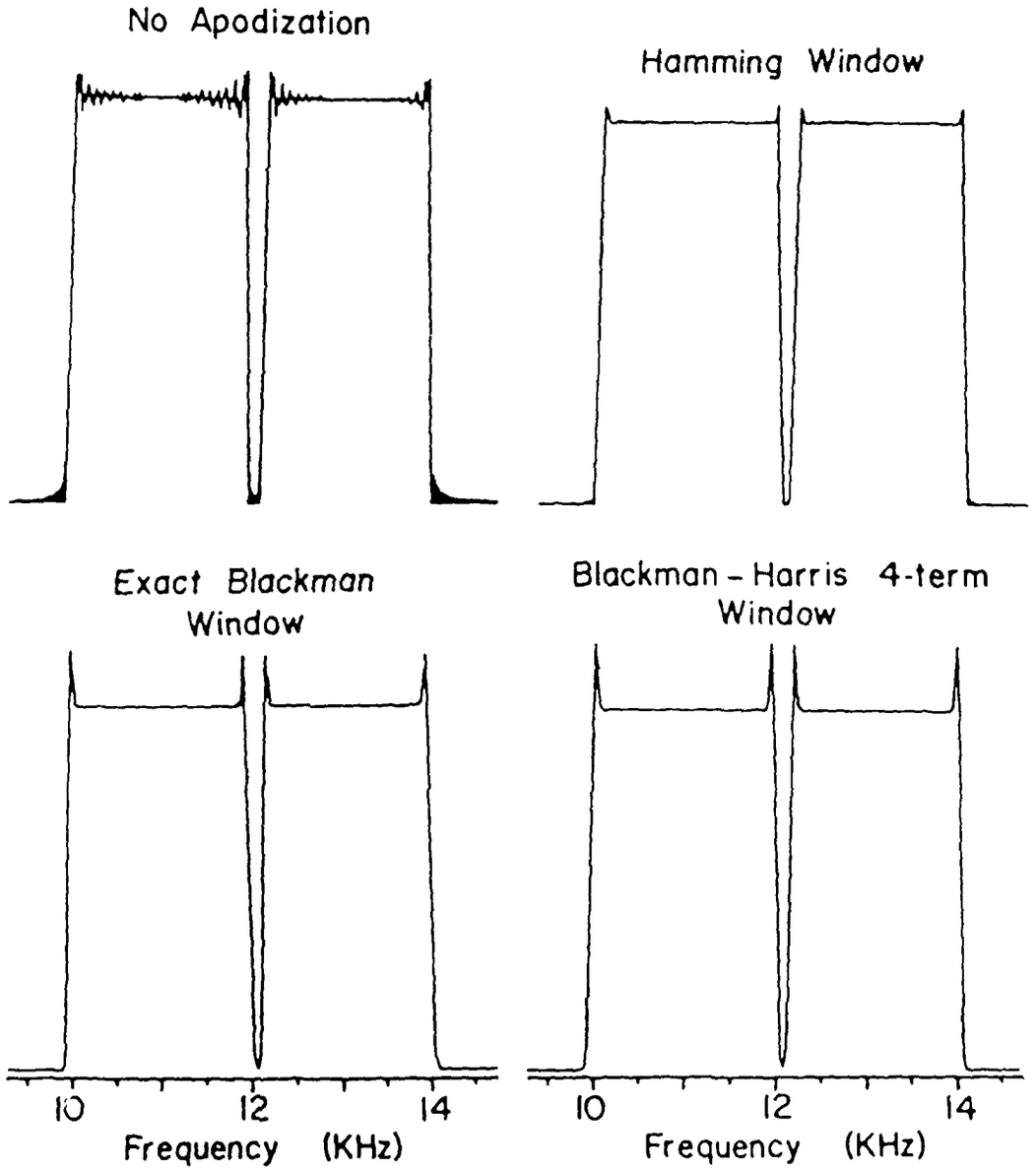
No Apodization
Hamming Window
Exact Blackman Window
Blackman - Harris 4-term Window
10
12
14
Frequency (KHz)
10
12
14
Frequency (KHz)

Figure 8

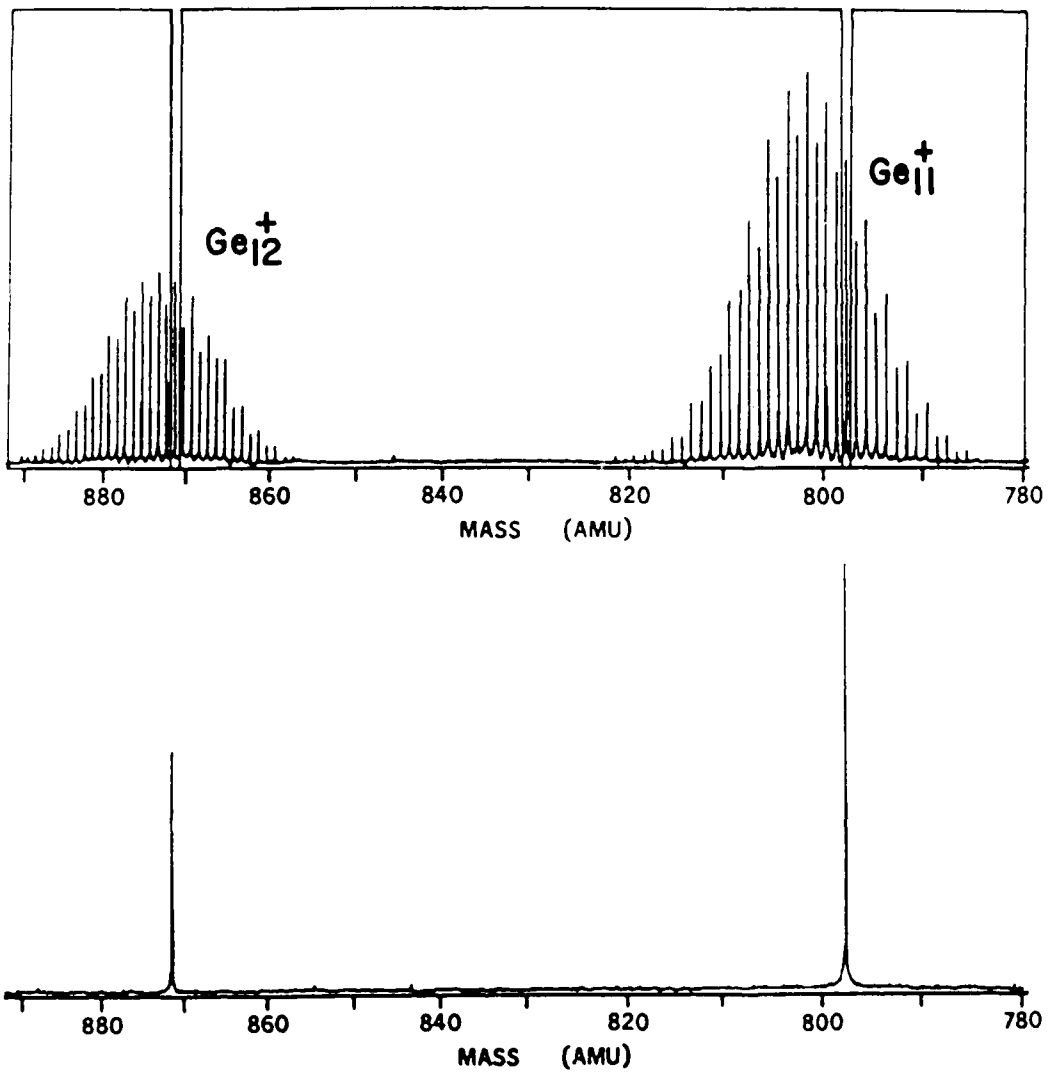
Ge_{12}^{+}
Ge_{11}^{+}
880
860
840
820
800
780
MASS (AMU)
880
860
840
820
800
780
MASS (AMU)

Figure 9

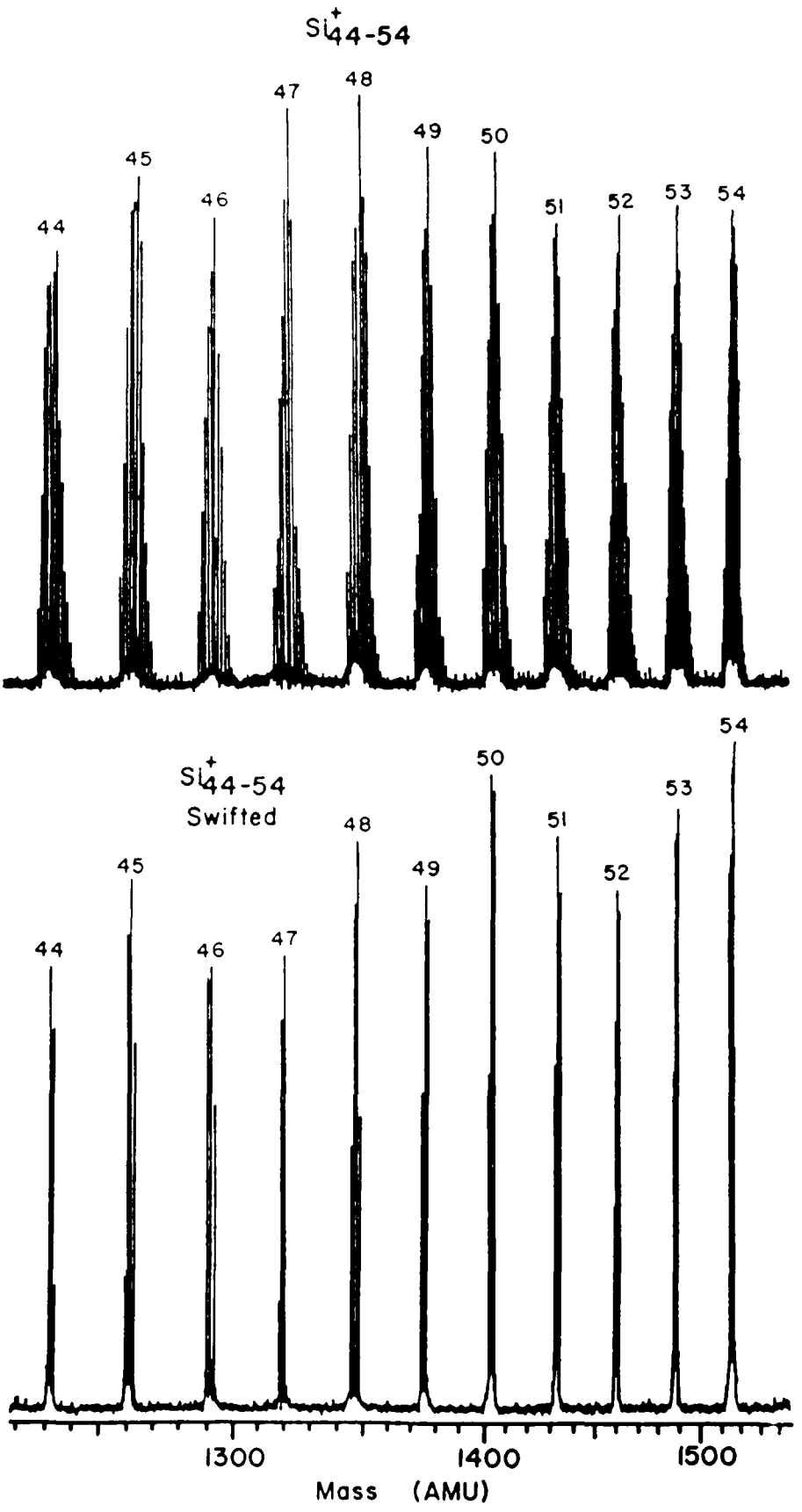
Si+44-54
44
45
46
47
48
49
50
51
52
53
54
Si+44-54
Swifted
1300
1400
1500
Mass (AMU)

Figure 10

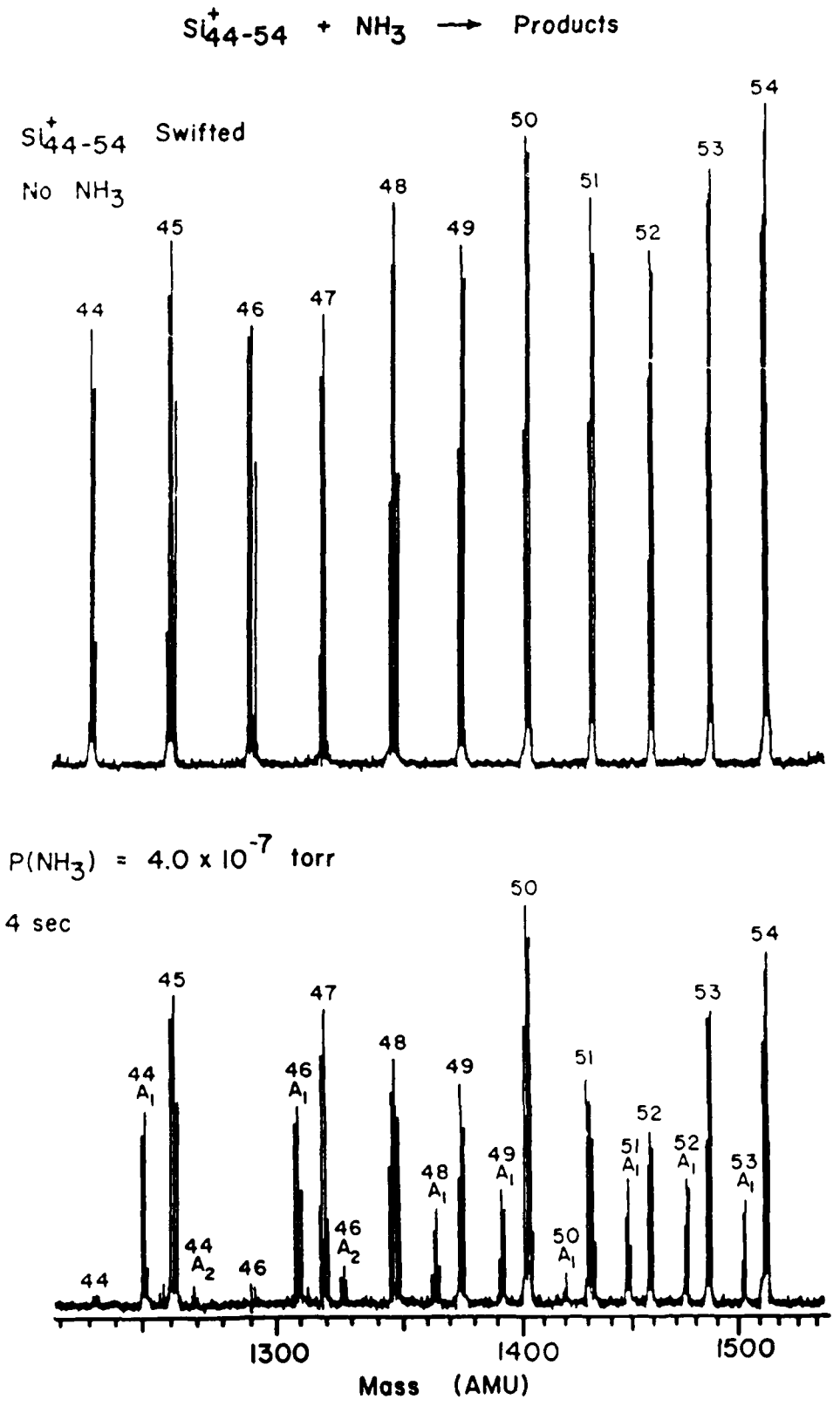
Si^+_{44-54} + NH_3 → Products
Si^+_{44-54} Swifted
No NH_3
44
45
46
47
48
49
50
51
52
53
54
$P(NH_3)$ = 4.0 x 10^{-7} torr
4 sec
44 A_1
44 A_2
46 A_1
46 A_2
48 A_1
49 A_1
50 A_1
51 A_1
52 A_1
53 A_1
1300
1400
1500
Mass (AMU)

Figure 11

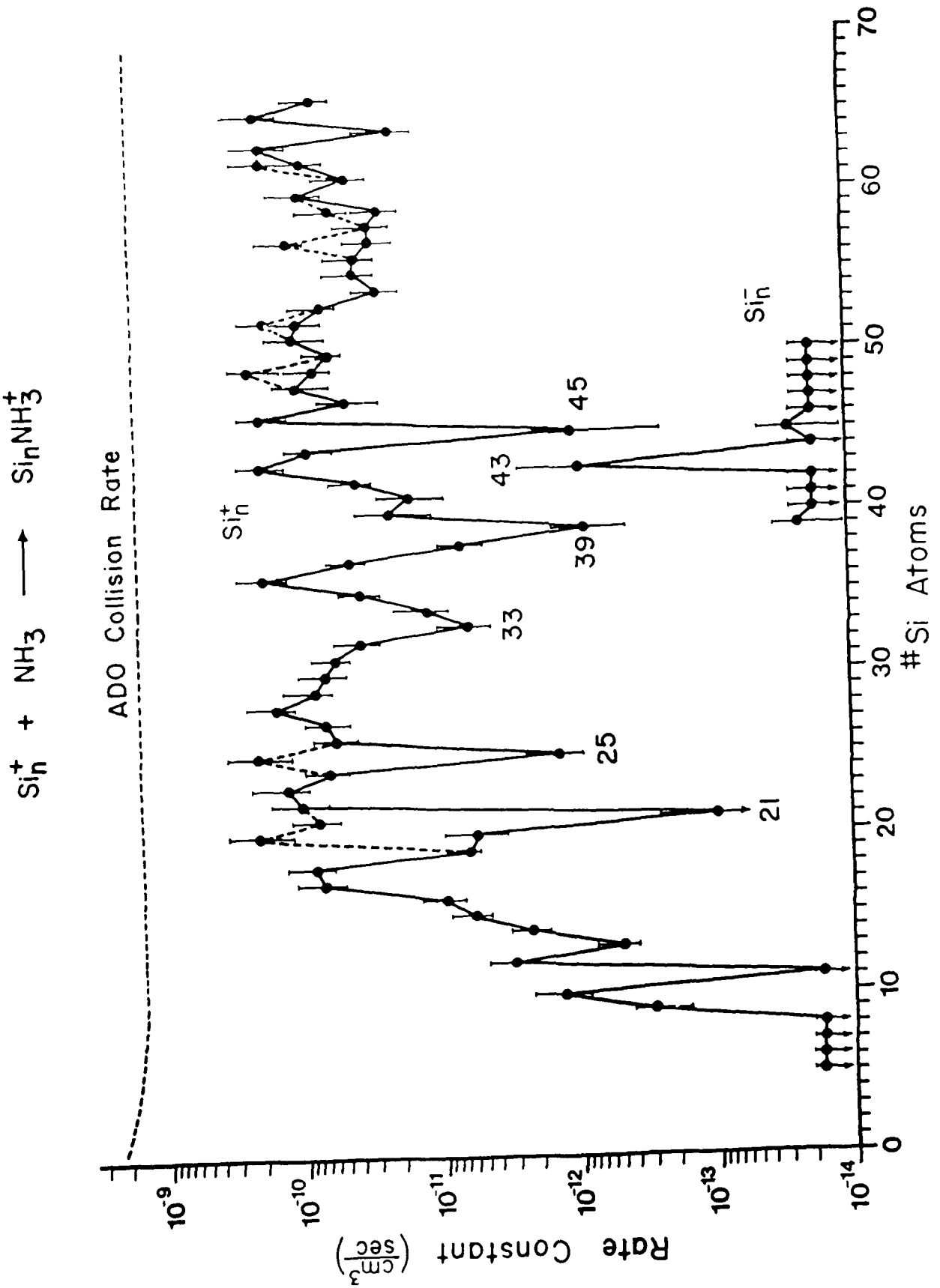
$Si_n^+ + NH_3 \longrightarrow Si_nNH_3^+$
ADO Collision Rate
Si_n^+
Si_n^-
21
25
33
39
43
45
Rate Constant $\left(\frac{cm^3}{sec}\right)$
10^{-9}
10^{-10}
10^{-11}
10^{-12}
10^{-13}
10^{-14}
0
10
20
30
40
50
60
70
#Si Atoms

Figure 12

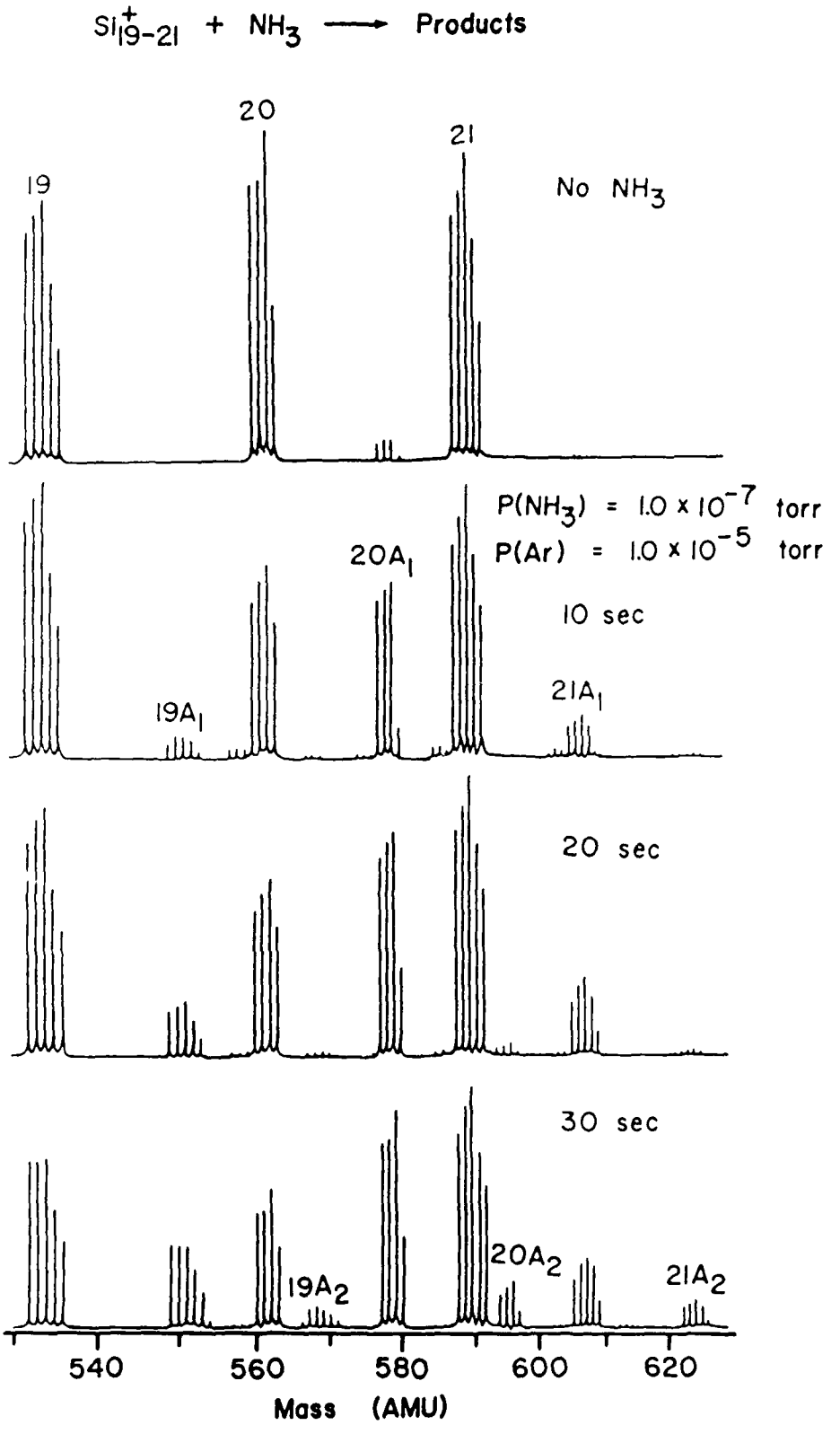
Si^+_{19-21} + NH_3 ⟶ Products
19
20
21
No NH_3
$P(NH_3)$ = 1.0×10^{-7} torr
P(Ar) = 1.0×10^{-5} torr
$20A_1$
10 sec
$19A_1$
$21A_1$
20 sec
30 sec
$19A_2$
$20A_2$
$21A_2$
540
560
580
600
620
Mass (AMU)

Figure 13

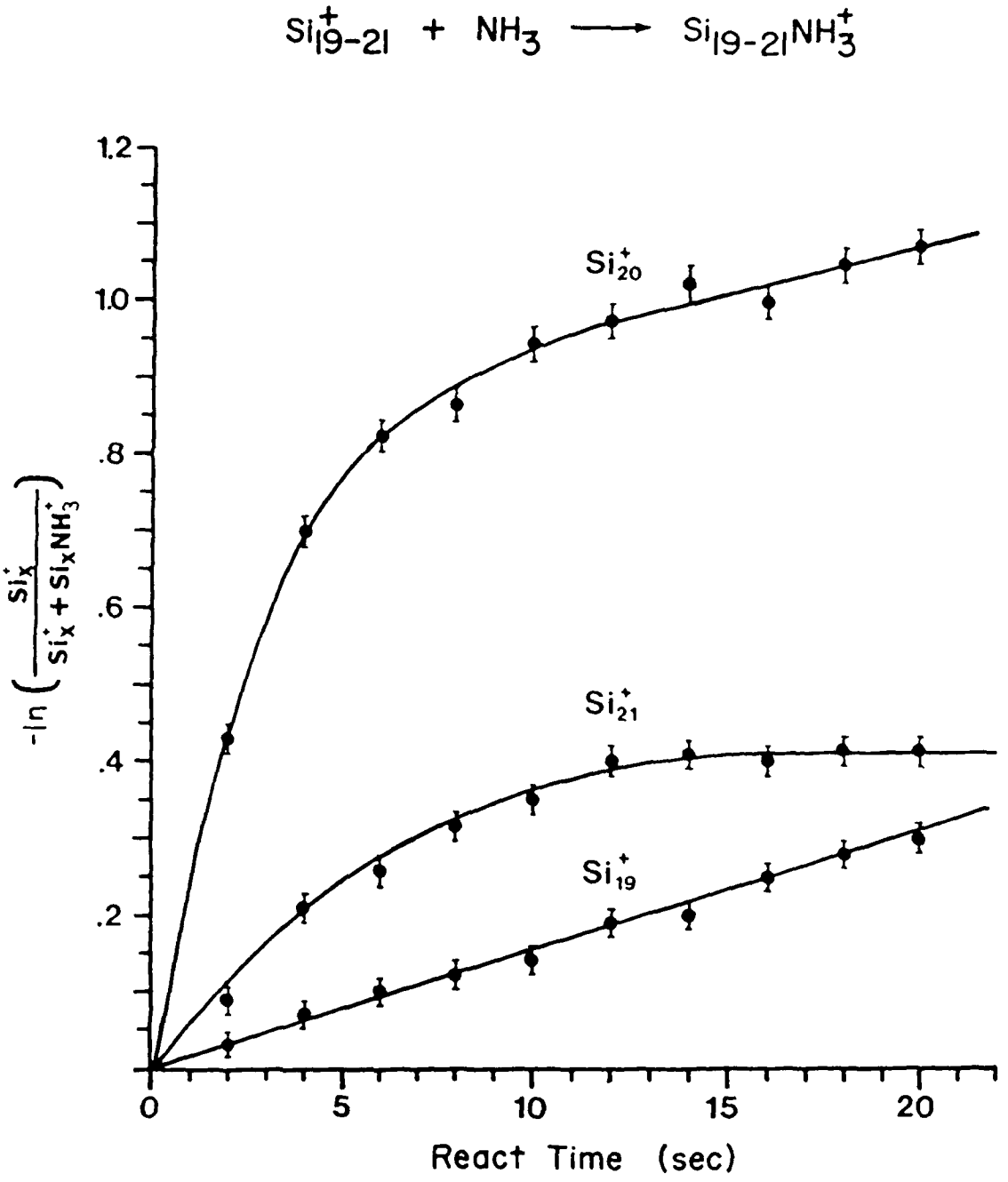
$Si^+_{19-21} + NH_3 \longrightarrow Si_{19-21}NH^+_3$
$-\ln\left(\frac{Si_X^+}{Si_X^+ + Si_XNH_3^+}\right)$
1.2
1.0
.8
.6
.4
.2
0
5
10
15
20
React Time (sec)
Si^+_{20}
Si^+_{21}
Si^+_{19}

Figure 14

Si_{45}

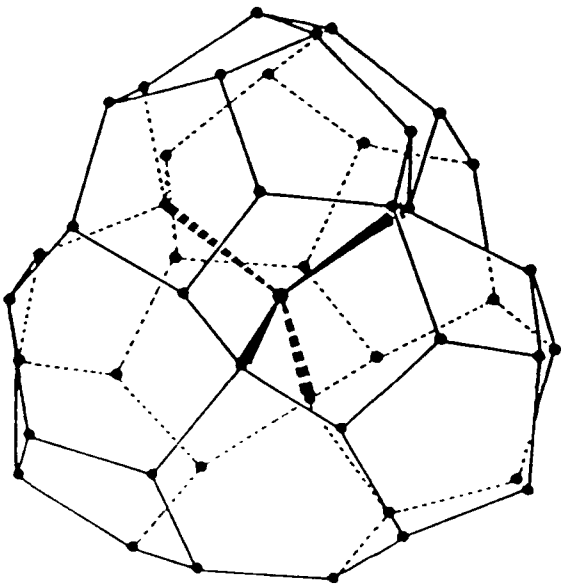

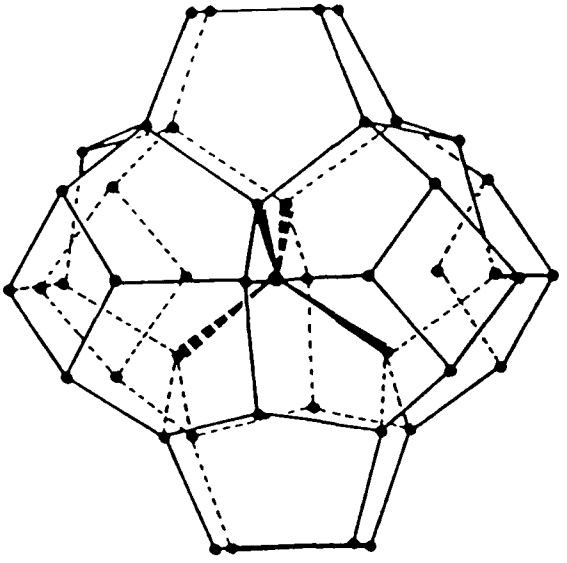

Figure 15